Vacuum 3D printing of highly filled polymeric matrix composites

Emanuele Alberto Slejko [a,1,*], Nicholas Sesto Gorella [a,1], Advenit Makaya [b], Paolo Gallina [a], Nicola Scuor [a], Stefano Seriani [a,**]

[a] DIA - Department of Engineering and Architecture, University of Trieste, Via Alfonso Valerio 6, Trieste, 34127, Italy
[b] ESA-ESTEC, Keplerlaan 1, 2200 AG, Noordwijk, ZH, the Netherlands

ARTICLE INFO

Keywords:
Additive manufacturing
In-orbit manufacturing
Surface energy
Outgassing
Thermal management
Polymer characterization

ABSTRACT

In this contribution, we have investigated how polymeric matrix composites for aerospace applications are affected, when fabricated at low pressure, by the additive manufacturing process. Commercial filaments have been selected based on their representativeness of materials derived from lunar resources. Standard samples of thermoplastic polymers reinforced by organic fibers and inorganic fillers have been printed inside a vacuum chamber, and their mechanical and thermal properties have been characterized and discussed based on the printing conditions. The reported study represents a preliminary investigation of the potential applicability of the 3D printing technology on highly filled polymers for extraterrestrial applications.

1. Introduction

Vacuum 3D printing represents an evolution of the typical additive manufacturing process, which is usually conducted in atmosphere and standard pressure. While vacuum printing finds, currently, limited interest for terrestrial applications (as no real benefits have already been observed to justify the complexity of the setup), it is a hot topic for the space sector. In fact, future exploration and colonization missions will require the capabilities to produce structures and mechanisms directly in-orbit or on-planet [1]. One such example is that of robotically operated bases set up during precursor missions intended for celestial bodies settlement efforts [2,3]. Indeed, the transportation of equipment and structures required for the settlement of an extraterrestrial base is impractical, under technological and economical points of view, when considering launching the material from Earth. Being able to print directly in vacuum has at least two advantages: 1) it forgoes the requirement of having a pressurized environment, which is a complex object with airlocks, active pressure regulation systems, power; 2) it enables very large structures to be printed. Printing in microgravity conditions has already been demonstrated: for example, the 3D printer inside the International Space Station works under a controlled atmosphere of 1 bar and 25 °C, thus, with the exception of gravity, representing the same environment in which terrestrial printers operate [4]. 3D printing not only represents a promising manufacturing technology for the development of structures in space, but also for the servicing of spacecraft in orbit and the increasing utilization of polymers for space applications [5–8]. Being able to demonstrate the reliability of 3D printing under vacuum, thus, can be a game changer for the development of efficient production processes in space.

While some notable works have recently been carried out on this topic, more experimentation is needed [9,10]. This is particularly true when the addition of In Situ Resource Utilization (ISRU) is considered as a critical part of the manufacturing process. In fact, the challenge relies not only in being able to print under vacuum but, more importantly, doing so recurring to a high portion of raw material already present in the target environment (the Moon, Mars, etc.) [11–13]. This would allow optimal exploitation of resources for the production of infrastructures and mechanisms, without recurring to transport the raw materials from Earth's gravity well [14]. While extremely important from a technological perspective for a sustainable presence of humans on the surface of other planets, this aspect is also economically fundamental in promoting a fast progress towards the realization of technology demonstrators and prototypical missions.

Regolith-based concrete is one of the most investigated construction materials to be used on the Moon; unfortunately, its processing is, usually, extremely energy-intensive [15–17]. 3D printed composites based on polymeric material, instead, present the advantage of being easily processable and manufacturable in complex geometries, with several

* Corresponding author.
** Corresponding author.
E-mail addresses: easlejko@units.it (E.A. Slejko), sseriani@units.it (S. Seriani).
[1] these authors contributed equally.

studies focusing on the influence of the printing conditions and the filler ratio on the final properties of materials printed under standard pressure [18,19]. Furthermore, the amount of filler can reach high ratios, representing a valid option for the utilization of in situ resources. For example, regolith powder can be added to polymeric matrices to confer strength, hardness and shielding properties to the materials [20].

Organic fibers may also represent an alternative reinforcement for polymeric matrices, as long as they derive from the agricultural activities implemented for sustainable human life on an extraterrestrial planet. Some preliminary investigations have been conducted on the possibility to grow and cultivate plants in space, with some promising indications for the future development of this technology [21,22].

Investigating the effects of vacuum-printed composites on the properties of printed parts represents a promising topic for potential advanced terrestrial applications, too. If higher resolutions and enhanced accuracies could be demonstrated while low pressure printing, sectors like the biomedical and the automotive would greatly benefit from these improved features. One limitation of manufacturing under vacuum is related to the dimensions of the object to be produced: large objects require extended volume and, thus, very large and expensive vacuum chambers. It is worth noting that 3D printing technique carries itself the constraint of a limited size for the printed part, as the building volume is usually fixed. Nonetheless, the application of vacuum could benefit small objects from potential defects due to, for example, an uneven distribution and transfer of heat and the presence of air impurities inside the printed object [23,24].

In this contribution, we have investigated the reliability of the 3D printing process of highly filled polymers when operating at low pressure. The need for commodity thermoplastics as main materials for this research is due to the constraints in thermal management of the available experimental setup. While the mechanical performance of commodity thermoplastics is not comparable with high-end polymers like poly(ether ether ketone) or polycarbonate (PEEK and PC, respectively), the thermal control in the low pressure chamber would be much easier to manage. Furthermore, considering the critical role of ISRU for space exploration, in the present study we have performed the analysis of the fabrication process on polymeric matrices filled with high contents of organic or inorganic reinforcements. The necessity of reliable and efficient manufacturing systems for the exploration of other planets demands the exploitation of novel manufacturing techniques and conditions. This research aims to close the gap between our current understanding of the additive manufacturing techniques and the application of such fabrication process in harsh environments, like the surface of the Moon, by evaluating the performance of vacuum 3D printed products. The main objective of this work is the investigation of the effects of printing in a low pressure environment on highly filled polymeric samples and the potential future adoption of this technique for advanced applications in space.

2. Materials and methods

2.1. Materials

Three commercial filaments have been purchased and used throughout this research: PLA, PLA filled with 40% organic fibers (pine wood fibers) and PLA filled with 50% inorganic clays. All filaments are PLA-based, with the addition of an impact modifier (not specified by the manufacturer). These highly filled filaments have been selected as representatives of plant-based materials reinforced with large amounts of lunar resources. There are not many products, commercially available, with such high fiber-to-matrix ratios. Another unique trait of these materials is related to the common methodologies to infer their mechanical properties: these methodologies prove to be useful for materials with ratios of fiber-to-matrix which are generally far from that of the materials we have considered in this study [25–27].

2.2. Conditioning of filaments

Although there is no proper standard defined for the storage conditions of polymer filaments used in 3D printing, we have based this profile to be conservative with respect to industrial practice. Indeed, manufacturers typically suggest keeping humidity-affected polymers at relative humidity levels below 50% when not in use, and recommend keeping the material in open air for the shortest time possible. It is well know that water-swollen filaments results in poor performance finished parts, characterized by bubbles and poor adhesion [28]. To limit the content of humidity inside the material, all filaments, at least for 24 h and before further processing or testing, have been stored in a dry box containing silica gel with relative humidity lower than 10%.

2.3. 3D printer specifications

The printer chosen to operate under vacuum conditions is the Monoprice Select Mini V2, Fig. 1a and b. This printer has been chosen mainly due to its small size and its all-metal construction. The main characteristics of the printer are shown in Table 1.

However, due to the dimensions of the vacuum chamber (400 mm in diameter and 250 mm in depth), some modifications to the printer were needed.

2.4. 3D printer adaptation to vacuum chamber

The printer used for fabrication was modified to fit into the vacuum chamber and to operate properly under the different working conditions (pressure as low as 10^{-4} bar). To meet the first requirement, i.e. accommodating the printer inside the vacuum chamber, the extruder motor has been relocated from the top of the printer. To adapt the printer to the vacuum chamber working conditions, instead, the

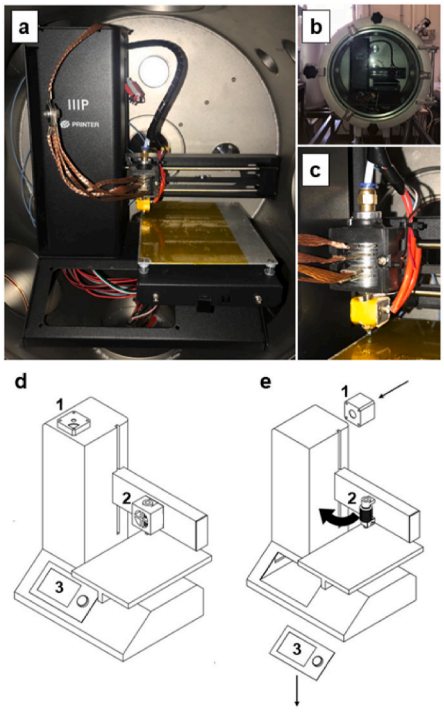

Fig. 1. Vacuum 3D printing setup: FDM Printer inside the vacuum chamber (a); overall view of vacuum 3D printing setup (b); detail of the printer hot end: cooling fan has been removed while copper thermal braids are applied instead (c). Printer schematic view before modifications (d). Printer schematic view after modifications (e): repositioning of the extruder motor (1), removing of cooling fan and substitution with copper braids (2) and removal of control interface and control board from the printer body (3).

Table 1
Monoprice Select Mini V2 main characteristics, as found on the manufacturer's website at the link: https://www.monoprice.com/product?p_id=21711.

Characteristic	Value
Build Volume	120 × 120 × 120 mm
Resolution	100–300 μm
Filament Diameter	1.75 mm
Nozzle Diameter	0.4 mm
Hot-end Setup	Bowden
Max. Print Speed	55 mm/s
Max. Extruder Temperature	250 °C
Max. Build Plate Temperature	60 °C

extruder cooling fan and its support have been replaced with a conductive-type cooling system. Specifically, four copper braids have been applied; they connect the cooling fins of the extruder to the metal body of the printer (Fig. 1c). Furthermore, the control interface and control board have been removed from the printer body and located externally to the vacuum chamber, allowing control of the printer once the chamber has been locked. The main modifications are schematically shown in Fig. 1d and e. Using a D-type vacuum-proof electrical feedthrough it was possible to connect the external control system to the printer itself. Finally, in order to achieve the lowest degree of vacuum allowed by the pumping system, all unnecessary materials have been removed. In particular, the polymeric sheet covering the printing plate was replaced with a layer of Kapton®, and excess lubricating grease has been eliminated from the prismatic joints controlling the axes of the printer.

2.5. Thermal imaging setup

The heat exchange and dissipation from the extruder hot-end is an important phenomenon that needs to be kept under control when printing in vacuum. As such, an infrared sensitive camera was implemented in the experimental setup, as reported in Fig. 2a–c. A Germanium viewport was designed and implemented, thanks to its transparency to the wavelengths typical of IR emissions. The viewport window is a Ge monocrystalline optical disk with a diameter of 25 mm and a thickness of 2 mm; it has a transmission range between 7 and 11 μm.

2.6. Printing conditions

The setup in Table 2 has been selected taking into account the manufacturer's recommendations regarding print temperature and print speed. Layer height has been chosen based on relevant literature concerning the effect of printing parameters on PLA-reinforced composites [29,30]. To obtain a performant final product, an infill density of 100% has been selected. Finally, special attention was given to the temperature of the printing plate, here set at 45 °C instead of 60 °C. This is related to the fact that the absence of convection made the printed sample too soft, negatively affecting the print quality. Lowering the build plate temperature gave the sample the required mechanical stability in order to sustain the subsequent layers and maintain good dimensional stability. The pressure profile during a single vacuum print is reported in Fig. 2d. It has been observed that the minimum pressure achieved through the printing process usually decreases as the number of prints increases (see Figure SI1): this is probably given by the outgassing of the printer lubricants that can be found on the prismatic joints and motors.

2.7. Characterizations

Granulometry Analysis: Inorganic clays have been characterized in terms of size and shape. PLA filled with clays has been thermally

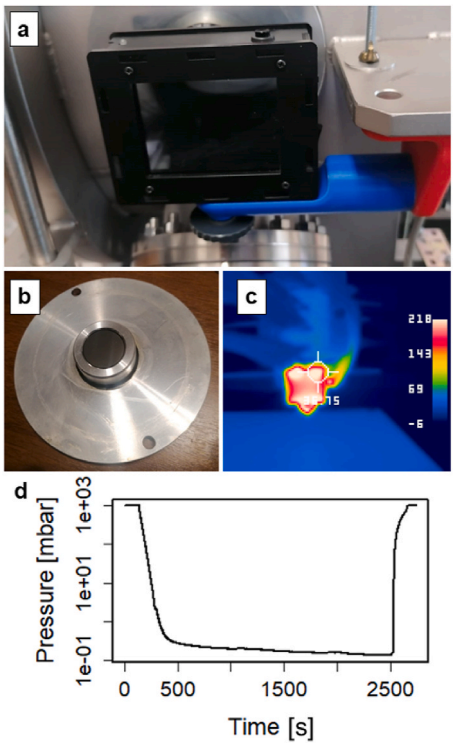

Fig. 2. Vacuum 3D printing setup. Thermal camera correctly placed in front of the Germanium viewport (a). Detail of the germanium viewport (b). Thermal image captured by IR camera during printing phase (c). Pressure profile during vacuum printing: the pressure profile rapidly decreases after pump activation and is maintained constant during the printing phase. Finally, the pressure rises due to the opening of the vent (d).

Table 2
Printing setup for atmospheric and low pressure printing, based on recommendations found on the manufacturer's website www.formfutura.com.

Parameter	Value
Layer Height	0.175 mm
Wall Thickness	1.05 mm
Infill Density	100%
Printing Temperature	215.0 °C
Build Plate Temperature	45.0 °C
Flow	100%
Print Speed	50 mm/s

decomposed at 800 °C for 1 h, the remaining powder has been collected and analyzed to the optical microscope and by x-ray diffractometry.

Mechanical: Ultimate strength, modulus and elongation at break have been evaluated via uniaxial tensile tests, performed with a Shimadzu AGS-X test machine equipped with a 10 kN load cell. Three samples for each experimental condition have been prepared, and tests were conducted according to ASTM D638-03 (Figure SI2).

Thermal: To investigate the thermal behavior of the materials, Differential Scanning Calorimetry (DSC) has been performed with a Netzsch DSC 200 F3 Maia instrument. 5 mg of material has been collected from filaments and 3D-printed samples and heated, inside aluminum crucibles, from 25 to 210 °C with a rate of 10 °C•min^{-1}. Thermogravimetric analysis (TGA) was performed in order to characterize the thermal stability of the materials. 5–10 mg of material has been placed in alumina crucibles and heated with a Netzsch STA 409 EP instrument, from 30 to 600 °C, with a heating rate of 10 °C•min^{-1} in air or argon flux [31].

XRD: X-ray powder diffraction patterns were recorded using a

Bruker-Axs (Siemens) D5000 X-ray diffractometer with Cu-Kα radiation. The powder was placed on an aluminum plate for measurement.

3. Results and discussion

3.1. Representativeness of starting materials

The inorganic clay powder (micrograph reported in Fig. 3a) has been characterized in terms of size and shape, and results have been compared to the available data for lunar regolith [32]. The composition of the inorganic filler, as obtained by x-ray diffractometry, indicates it is mainly $CaSiO_3$ and is shown in Fig. 3b. Calcium and silicon compounds are quite common on the lunar surface; the filler, thus, has been selected for its high representativeness, in terms of chemical composition, of material that can be obtained and processed from the lunar environment. Furthermore, we have found that the mean characteristic size of the PLA filler is 9.3 μm, with an average aspect ratio of 0.14 (Fig. 3c and d). While the size value can be found in the smaller-size portion of lunar regolith samples (which usually presents a size range of 7–500 μm), the PLA filler is more elongated than regolith (aspect ratio of 0.55). Nevertheless, the clay filler in this study can be indicated as fairly representative of inorganic clays derived from lunar soil.

We have performed an analysis of the composition of the pine wood filler for potential matching of organic material grown on the Moon. The only reference available, at the best of our knowledge, is the Chinese experiment performed by the Chang'e−4 spacecraft in 2019 [33]. It is reported that two leaves of cotton have grown on the Moon surface, indicating a potential for agricultural activities on our natural satellite. The composition (in terms of cellulose, hemicellulose, and lignin content) of the cotton stalk is similar to pine wood, indicating pine wood fibers as a good representative of organic material grown in the lunar environment (Fig. 3e).

3.2. Characterization of samples

The comparison of the mechanical properties of filled materials indicates that there are no major differences between atmospheric pressure and low pressure printed samples (Fig. 4). Furthermore, the low mechanical performance of filled PLA, when compared to reference values [34], can be related to the presence of a compatibilizer to promote a better miscibility and workability of the highly filled polymers. It is worth mentioning that, especially for 3D printing filament, a large variation of properties values is often observed due to slightly different content of additives or potential blending to improve flow rate of the material during printing. Irrespective of the absolute values of the starting materials, no sensible change in the mean values of the observed properties is reported when moving from atmospheric printing to low pressure fabrication.

The negligible impact of vacuum printing compared to atmospheric printing on the composition and properties of highly filled PLA is indicated by Fourier Transform Infrared Spectra as well. As can be seen in Fig. 5, no sensible difference is observed in the fingerprint region of the materials when comparing printed samples. It is possible to deduce, then, that the chemical composition of the material is preserved during the processing, irrespective of the printing conditions (in terms of environment pressure). In the fingerprint region of filled samples, furthermore, characteristic peaks are observed which are not linked to PLA; the main ones are located at 1154 and 1723 cm^{-1} (see Figure SI3). We suppose they are related to the second component mixed with PLA and we believe it could be poly (butylene succinate-co-adipate), PBSA, as these two peaks are consistent with its characteristic spectrum [35]. We believe that PLA has been mixed with different amounts of PBSA in the filled materials to promote compatibility between the matrix and the fillers. Furthermore, it is well known that PBSA is an impact modifier for PLA, improving its toughness and workability [36,37].

Thermal characterization of pristine filaments and printed parts present different behavior upon atmospheric or vacuum printing. Differential scanning calorimetry curves in Fig. 6a,b,c show the typical T_g and T_m of PLA at 63 °C and 154 °C, respectively. Unfilled PLA presents a cold crystallization in the range 100–105 °C; at this temperature polymer chains start to rearrange and an exothermic peak is detected. In addition, filled polymers display an endothermic peak centered at 88 °C, which is associated with the presence of PBSA in the blend. It has been reported that poly(butylene succinate-co-adipate) presents a melting temperature in the range of 80–100 °C, thus consistent with the observed endothermic peak [35]. The occurrence of a cold crystallization in filled polymers is unclear due to the presence of the melting peak of PBSA. Comparing the curves in Fig. 6, we can state that no differences

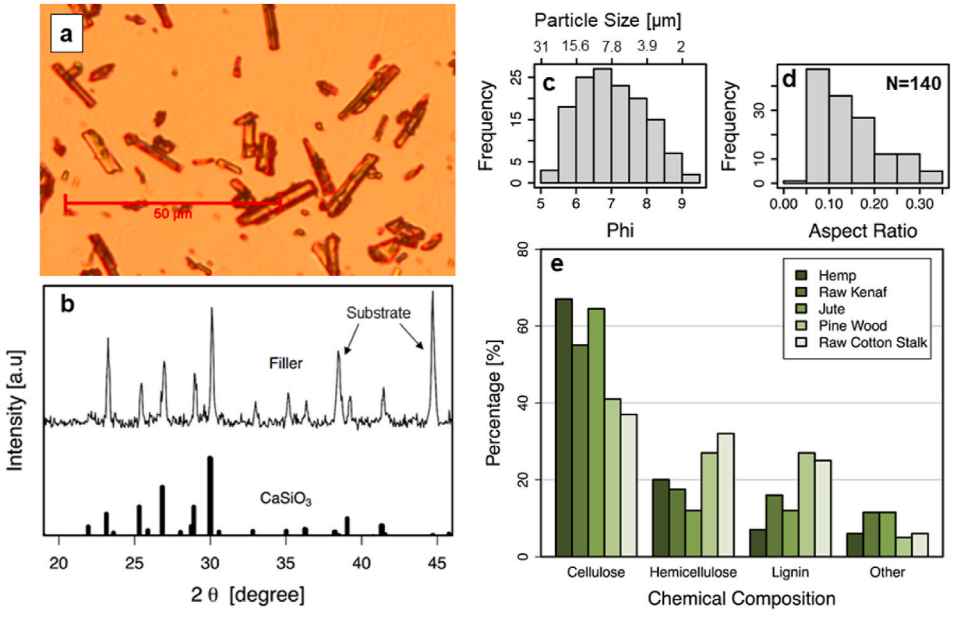

Fig. 3. Characterization of inorganic filler: micrograph of inorganic clays (a). XRD pattern of PLA filler and $CaSiO_3$ (b); the intense peaks at 38 and 44 degree are related to the aluminum plate. Size distribution (c) and aspect ratio (d) of inorganic clays, as obtained by analysis of micrographs for N = 140 particles. Composition of the main organic fibers of PLA (e): pine wood presents a similar composition to raw cotton stalk. Values are reported in Table SI1.

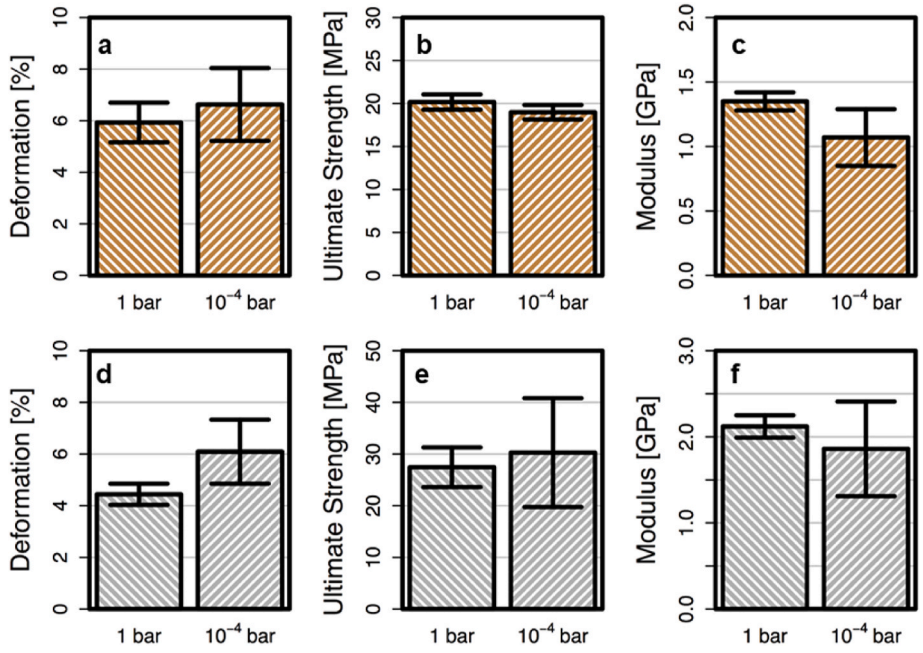

Fig. 4. Mechanical properties of filled-PLA printed under atmospheric pressure (1 bar) and low pressure (10^{-4} bar). Deformation (a), ultimate strength (b) and modulus (c) of wood-filled PLA. Deformation (d), ultimate strength (e) and modulus (f) of clay-filled PLA.

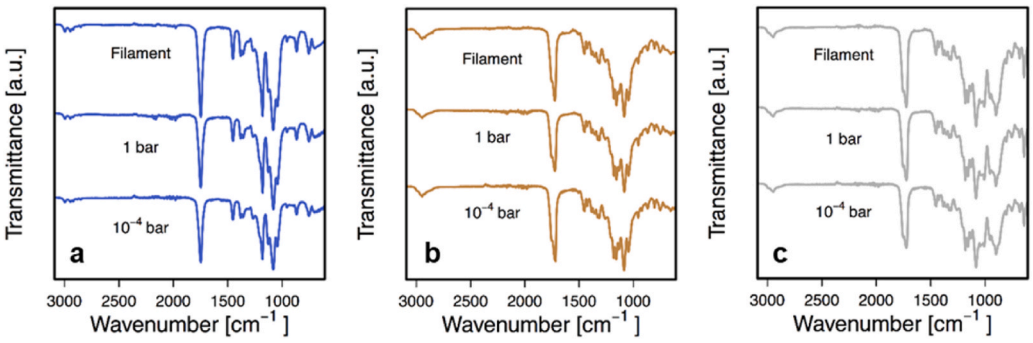

Fig. 5. FTIR spectra for pristine filaments, samples printed under standard pressure (1 bar) and samples printed under low pressure (10^{-4} bar) of PLA (a), wood-filled PLA (b) and clay-filled PLA (c).

are observed, regarding the printing conditions, in terms of thermal transitions. The crystallinity of samples is measured as the area of the melting peak in DSC curves minus the eventual cold crystallization. The total crystallinity X_c has been evaluated by the formula:

$$X_c = \frac{X_{PLA}\varphi_{PLA} + X_{PBSA}\varphi_{PBSA}}{\varphi_{PLA} + \varphi_{PBSA}}$$

$$X_{PLA} = \frac{\left(H_{m,PLA} - H_{cc,PLA}\right)}{H^0_{m,PLA}} * 100$$

$$X_{PBSA} = \frac{\left(H_{m,PBSA} - H_{cc,PBSA}\right)}{H^0_{m,PBSA}} * 100$$

where H_m and H_{cc} are the enthalpy of fusion and cold crystallization, respectively, and Φ represents the weight fraction of the component. The standard enthalpies of fusion, H^0_m, are referred to 100% crystalline PLA or PBSA and are equal to, respectively, 93 J/g or 142 J/g. Fig. 6d,e,f show the measured crystallinity of filaments and printed samples. It can be observed that, for all three compositions, there is no substantial change in the values of crystallinity for printed specimens. It has been reported how, for high resolution printing, the conduction heat transfer plays a crucial role in cooling printed parts, reaching cooling rates in the order of 200 °C/s [10]. As the layer thickness for our sample is 0.175 mm, we expect the layer temperature gets below the glass transition temperature in a very short time. This is coherent with the reported values of crystallinity: both atmospheric and low pressure printed parts cool down almost immediately; thus, the amount of crystal phase formed in both datasets is similar. This observation, furthermore, suggests that, as long as the resolution of the printing is high (i.e. thin layers), the heat transfer is not sensibly influenced by the reduction of the convection mechanism when printing under low pressure.

The calculated values of crystallinity are coherent also with the reported mechanical properties of samples, which do not indicate any consistent deviation when comparing atmospheric and low pressure printed parts. It is worth noting how the standard deviation of measured values increases when printing at 10^{-4} bar. We believe this is caused by an accumulation of heat during consecutive production of samples, which results in different temperature gradients within printed parts and, consequently, a broader distribution of observed values of crystallinity and mechanical properties. This outcome can be controlled by tailoring the amount of heat dissipation through conduction.

Fig. 7 shows the thermal degradation in air of pristine filament and samples printed at different pressures. Data for unfilled PLA presents one

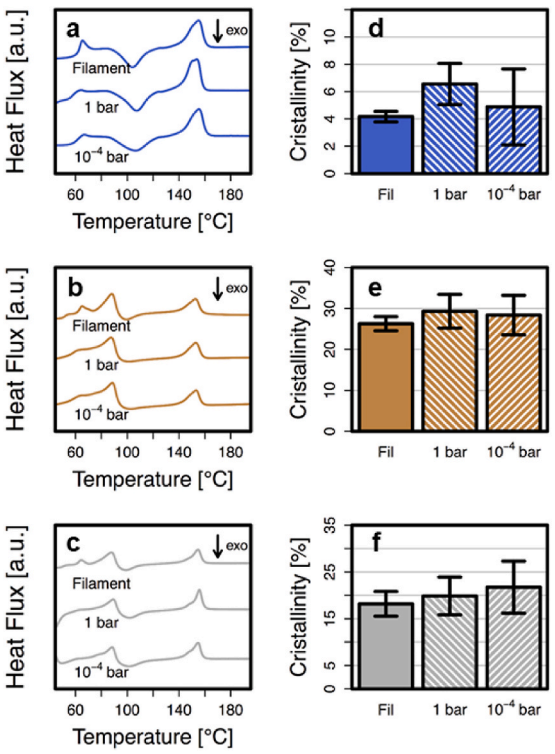

Fig. 6. Differential scanning calorimetry analysis of filament and printed parts for PLA (a), wood-filled PLA (b) and clay-filled PLA (c). Relative crystallinity for PLA (d), wood-filled PLA (e) and clay-filled PLA (f). Values of the crystallinity are reported in Table SI2.

single degradation stage for all samples, identified by one peak of the derivative thermogravimetry (DTG) (Fig. 7a,b,c). Filled materials, instead, present a more complex behavior, with three different steps of weight loss (and three corresponding peaks of DTG, see Fig. 7d,e,f,g,h,i). As can be seen from Fig. 8a and b, the first stage of the thermal degradation in air is associated with the decomposition of PLA, which takes place on average at 352 °C and results in the almost complete degradation of the material (−94.3% mean weight loss). The decomposition of PLA happens at lower temperature in filled samples, and it is followed by a second transition that takes place in the range of 377–381 °C (Fig. 8c,e) for both wood-filled and clay-filled PLA (−28.7% and −21.3% weight loss, respectively; Fig. 8d,f). This second transition is associated with the presence of PBSA in the blend and, for wood-filled PLA, to the degradation of cellulose and hemicellulose in the organic filler. It is well documented in the literature that the thermal degradation of PBSA occurs around 375 °C, which is quite consistent with the observed second peak [37]. Furthermore, the clear presence of this peak in the thermogravimetric curves may indicate that the two polymers have formed immiscible phases, an event quite common due to unfavorable thermodynamics of mixing [36]. This is supported by the constant observed value of the glass transition temperature, which is around 63 °C for all samples as can be seen in Fig. 6.

When TGA is conducted in air, a third transition takes place. For atmospheric printed samples, the third degradation is observed at 480 °C and 428 °C (wood-filled and clay-filled PLA, respectively) while, for pristine filament and samples printed at low pressure, this transition occurs at 518 °C and 457 °C (for wood-filled and clay-filled PLA, respectively), see Fig. 8c,e. The mass change during the final transition is, on average, −9% and −3% for wood-filled and clay-filled PLA (Fig. 8d,f).

When thermogravimetric analysis is conducted under argon flux, the third transition disappears. Fig. 9a,b,c,d presents the comparison of TGA for clay-filled PLA (which is not affected by the decompositions of organic fillers like wood-filled PLA) under air or argon flux. Based on

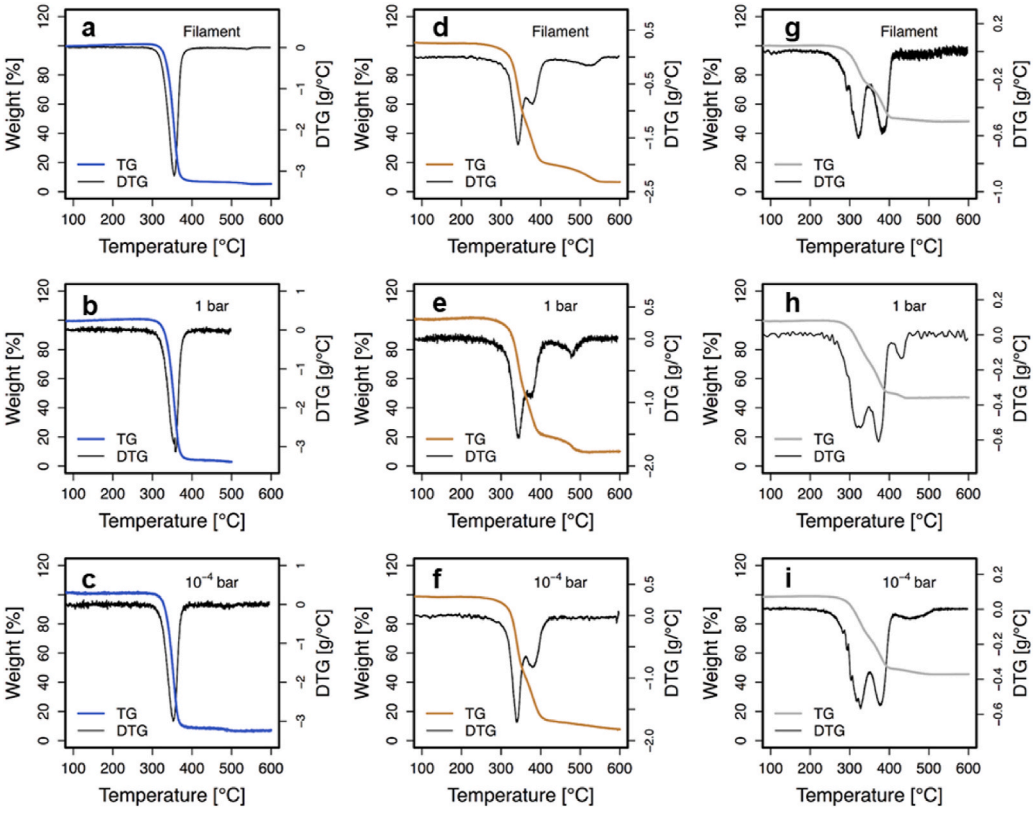

Fig. 7. Weight loss in air and derivative thermogravimetric analysis of filament and samples printed under different pressures.

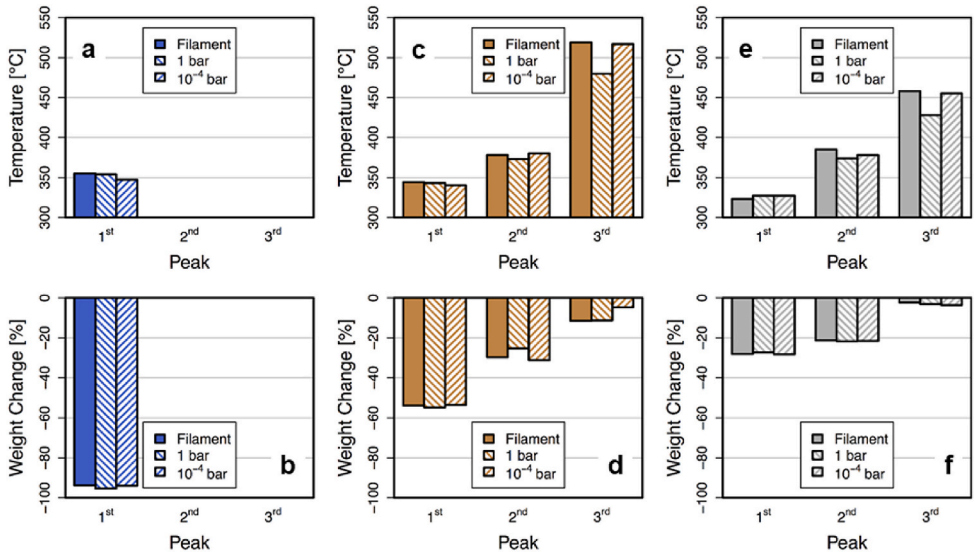

Fig. 8. Degradation temperatures and weight loss occurring during the three decomposition stages as observed in TGA under air for PLA (a and b), wood-filled PLA (c and d) and clay-filled PLA (e and f).

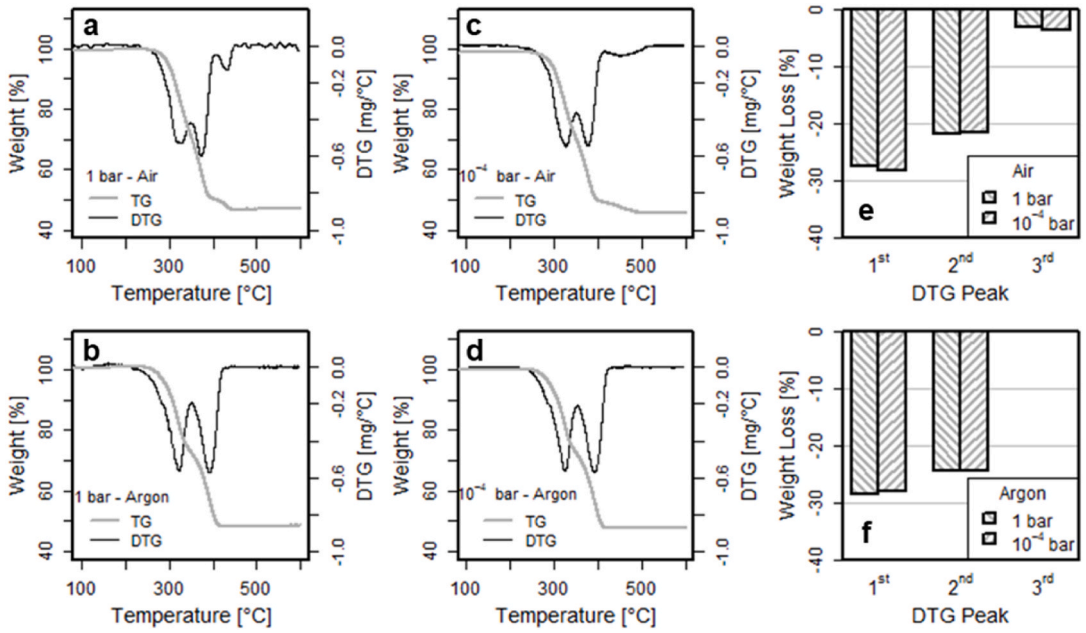

Fig. 9. TG and DTG analyses of clay-filled PLA. Sample printed under standard pressure and tested in air (a); sample printed under standard pressure and tested in argon (b); sample printed under low pressure and tested in air (c); sample printed under low pressure and tested in argon (d). Weight loss for the air-heated (e) and argon-heated (f) samples.

these results, we believe the third transition for air-heated samples results from oxidation and formation of volatile compounds of PBSA. At the temperatures upon which this reaction occurs, the PLA has already completely degraded: in fact, the weight lost during the first transition ($T < 350$ °C) is the same for both air and argon heating, indicating that PLA fully decomposes during this first reaction (Fig. 9e and f). Therefore, the third decomposition in air-heated tests must be related to the degradation of oxidized PBSA [38]. As further evidence of this, it is worth mentioning that the residual weight percentage at 600 °C is the same for both air-heated and argon-heated samples (47.3%), representing the percentage of the inorganic filler inside the material.

The dimensional accuracy of printed parts, instead, seems to be strongly influenced by the printing conditions. Fig. 10a and b report the thickness and width of dogbone samples as measured in the neck region (Fig. 10c). As can be seen, samples present a thinner but wider neck when printed under low pressure. We speculate this could result from the larger value of the surface tension of the molten strand: in fact, it is known that the surface tension of materials increases if the environment pressure is reduced [39–41]. A larger value of the surface tension of the strand could represent the driving force for an enhanced wettability on the print bed as, for thermodynamic reasons, the filament material prefers a larger contact area with the substrate. This, in turn, would result in a thinner but wider deposited strand, represented in Fig. 10d and inset. As the material builds up to form the final geometry, this effect is summed up and a measurable deviation from the design dimensions is observed. We expect this behavior to be more severe the lower the chamber pressure during printing. As a consequence, this could represent a critical limitation of the process, if not appropriately addressed,

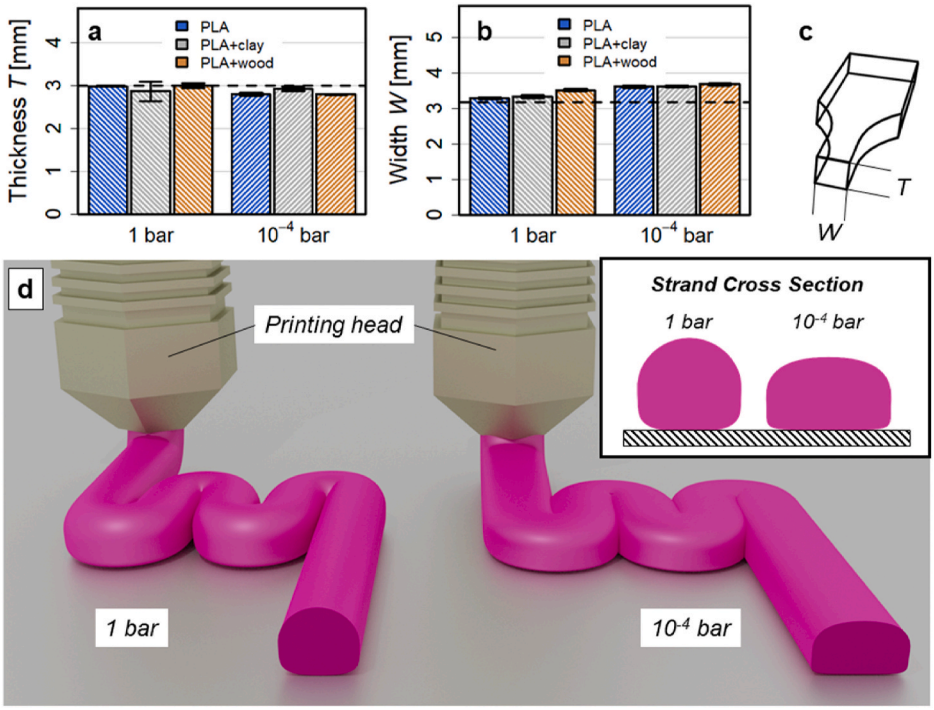

Fig. 10. Dimensional analysis of samples thickness and width (a and b); dashed lines indicate the design thickness and width, which are 3 mm and 3.18 mm respectively. Visualization of the measured quantities on a portion of the dogbone shaped sample (c). Representation of the potential difference in wettability, caused by the surface energies related to different pressure conditions, on printed strands (d).

especially when a high level of dimensional accuracy is required by printing under low pressure. In principle, this effect can be mitigated by compensative solutions during the design of the object; however, a systematic experimental analysis is needed to precisely determine the impact of the observed response.

3.3. Limitations of the present study

As mentioned in the introduction, in this study we have recurred to commodity thermoplastics (i.e. PLA) for the evaluation of the influence of the printing condition. This was due to the easier thermal management that can be applied in the processing of such materials inside a low pressure chamber. Obviously, advanced technological applications require the use of high-end materials. Nonetheless, the indications provided by our investigation and the observed effects of low pressure printing are expected to be of interest to other polymeric materials as well.

Regarding space applications, we can mention that, even if the composition of the fillers of this study was relevant, more realistic simulants are needed to conduct an accurate evaluation and technology demonstration. A second point to keep in mind is related to the level of vacuum: while no other study, to the best of our knowledge, has investigated the behavior of 3D printed polymers at pressure as low as 10^{-4} bar, the level of vacuum in the orbital regions around Earth and on the Moon is in the order of 10^{-10} - 10^{-11} bar. A high level of vacuum, however, could represent more an obstacle than a benefit for printing accuracy. In fact, if the pressure gets too low, chemicals could start boiling out of the filament, damaging it and lowering the quality of the printed parts. This could be a major drawback of the technology as it has been conceived at the present moment and more research is needed in this respect.

4. Conclusions

In this investigation, we have demonstrated that 3D printing can be conducted in a vacuum chamber with appropriate thermal control. Two different commercial highly filled PLA filaments have been printed at pressure as low as 10^{-4} bar; the quality of the material is not affected in terms of mechanical and thermal properties, as indicated by the characterization of standard samples. Instead, dimensional deviations have been observed for low pressure printed parts. This behavior can be related to the value of the surface tension of extruded strands, which is higher in a low pressure environment. As a result, the material tends to present a larger wettability on the substrate (or on the previously deposited layers), resulting in the observed wider but thinner samples. We believe this behavior is consistent with the printing conditions, therefore it represents a limitation to deal with when considering 3D printing of dimensional accurate products at low pressure. Regarding the 3D printing process itself, it has been shown that only minor modifications of commercially available desktop printers are sufficient to achieve good quality prints in vacuum. Heat dissipation can be effectively implemented via flexible copper thermal straps. The lack of the convection mechanism does not affect the quality of the part, as far as the cooling rate is high. We believe there is a critical value of the layer height at which the convection mechanism becomes dominant, but further investigation is needed in this respect. Other possible evolutions of this research rely on a more detailed parametric analysis of printing conditions and the use of high performance polymers like PEEK, for example. This study indicates that vacuum 3D printing could represent an interesting fabrication process for in orbit manufacturing and a fundamental asset for space exploration.

Funding

This research activity has been supported by ESA AO/2–1749/20/NL/GLC “OSIP Off-Earth manufacturing and construction campaign-study scheme”, part of the ESA’s Discovery program.

Declaration of competing interest

The authors declare that they have no known competing financial interests or personal relationships that could have appeared to influence the work reported in this paper.

References

[1] M. Moraguez, O. De Weck, Benefits of in-space manufacturing technology development for human spaceflight, in: IEEE Aerosp. Conf. Proc., 2020, https://doi.org/10.1109/AERO47225.2020.9172304.

[2] L. Mason, M. Rucker, Common power and energy storage solutions to support lunar and Mars surface exploration missions, Proc. Int. Astronaut. Congr. IAC-19-A5.1.8, (2019) 1–7.

[3] M. Kuhns, P. Metzger, Z. Hasnain, K. Zacny, Instant landing pads for lunar missions, in: Earth Sp. 2021 Sp. Explor. Util. Eng. Constr. Extrem. Environ. - Sel. Pap. From 17th Bienn. Int. Conf. Eng. Sci. Constr. Oper. Challenging Environ., 2021, pp. 1027–1032, https://doi.org/10.1061/9780784483374.094.

[4] T. Prater, N. Werkheiser, F. Ledbetter, D. Timucin, K. Wheeler, M. Snyder, 3D Printing in Zero G Technology Demonstration Mission: complete experimental results and summary of related material modeling efforts, Int. J. Adv. Manuf. Technol. 101 (2019) 391–417, https://doi.org/10.1007/s00170-018-2827-7.

[5] A. Flores-Abad, O. Ma, K. Pham, S. Ulrich, A review of space robotics technologies for on-orbit servicing, Prog. Aero. Sci. 68 (2014) 1–26, https://doi.org/10.1016/j.paerosci.2014.03.002.

[6] J.P. Randall, M.A.B. Meador, S.C. Jana, Tailoring mechanical properties of aerogels for aerospace applications, ACS Appl. Mater. Interfaces 3 (2011) 613–626, https://doi.org/10.1021/am200007n.

[7] I. Gouzman, E. Grossman, R. Verker, N. Atar, A. Bolker, N. Eliaz, Advances in polyimide-based materials for space applications, Adv. Mater. 31 (2019), https://doi.org/10.1002/adma.201807738.

[8] E.A. Slejko, A. Gregorio, V. Lughi, Material selection for a CubeSat structural bus complying with debris mitigation, Adv. Space Res. 67 (2021) 1468–1476, https://doi.org/10.1016/j.asr.2020.11.037.

[9] M. Quinn, U. Lafont, J. Versteegh, J. Guo, Effect of low vacuum environment on the fused filament fabrication process, CEAS Sp. J. 13 (2021) 369–376, https://doi.org/10.1007/s12567-021-00363-7.

[10] J. Zhang, B. Van Hooreweder, E. Ferraris, Fused filament fabrication on the Moon, JOM (J. Occup. Med.) 74 (2022) 1111–1119, https://doi.org/10.1007/s11837-021-05031-z.

[11] J. Carpenter, R. Fisackerly, B. Houdou, Establishing lunar resource viability, Space Pol. 37 (2016) 52–57, https://doi.org/10.1016/j.spacepol.2016.07.002.

[12] A. Meurisse, J. Carpenter, Past, present and future rationale for space resource utilisation, Planet. Space Sci. 182 (2020), 104853, https://doi.org/10.1016/j.pss.2020.104853.

[13] A.A. Altun, F. Ertl, M. Marechal, A. Makaya, A. Sgambati, M. Schwentenwein, Additive manufacturing of lunar regolith structures, Open Ceram 5 (2021), 100058, https://doi.org/10.1016/j.oceram.2021.100058.

[14] G.B. Sanders, W.E. Larson, Progress made in lunar in situ resource utilization under NASA's exploration technology and development program, J. Aero. Eng. 26 (2013) 5–17, https://doi.org/10.1061/(asce)as.1943-5525.0000208.

[15] M.Z. Naser, Extraterrestrial construction materials, Prog. Mater. Sci. 105 (2019), 100577, https://doi.org/10.1016/j.pmatsci.2019.100577.

[16] S. Lim, V.L. Prabhu, M. Anand, L.A. Taylor, Extra-terrestrial construction processes – advancements, opportunities and challenges, Adv. Space Res. 60 (2017) 1413–1429, https://doi.org/10.1016/j.asr.2017.06.038.

[17] T. Sik Lee, J. Lee, K. Yong, Ann, manufacture of polymeric concrete on the Moon, Acta Astronaut. 114 (2015) 60–64, https://doi.org/10.1016/j.actaastro.2015.04.004.

[18] M.R. Khosravani, F. Berto, M.R. Ayatollahi, T. Reinicke, Characterization of 3D-printed PLA parts with different raster orientations and printing speeds, Sci. Rep. 12 (2022) 1–9, https://doi.org/10.1038/s41598-022-05005-4.

[19] S. Pan, H. Shen, L. Zhang, Effect of carbon nanotube on thermal, tribological and mechanical properties of 3D printing polyphenylene sulfide, Addit. Manuf. 47 (2021), 102247, https://doi.org/10.1016/j.addma.2021.102247.

[20] C. Montes, K. Broussard, M. Gongre, N. Simicevic, J. Mejia, J. Tham, E. Allouche, G. Davis, Evaluation of lunar regolith geopolymer binder as a radioactive shielding material for space exploration applications, Adv. Space Res. 56 (2015) 1212–1221, https://doi.org/10.1016/j.asr.2015.05.044.

[21] N.O. Kozyrovska, T.L. Lutvynenko, O.S. Korniichuk, M.V. Kovalchuk, T. M. Voznyuk, O. Kononuchenko, I. Zaetz, I.S. Rogutskyy, O.V. Mytrokhyn, S. P. Mashkovska, B.H. Foing, V.A. Kordyum, Growing pioneer plants for a lunar base, Adv. Space Res. 37 (2006) 93–99, https://doi.org/10.1016/j.asr.2005.03.005.

[22] C. Zeidler, V. Vrakking, M. Bamsey, L. Poulet, P. Zabel, D. Schubert, C. Paille, E. Mazzoleni, N. Domurath, Greenhouse module for space system: a lunar greenhouse design, Open Agric 2 (2017) 116–132, https://doi.org/10.1515/opag-2017-0011.

[23] S. Wickramasinghe, T. Do, P. Tran, FDM-Based 3D printing of polymer and associated composite: a review on mechanical properties, defects and treatments, Polymers 12 (2020) 1–42, https://doi.org/10.3390/polym12071529.

[24] P.K. Penumakala, J. Santo, A. Thomas, A critical review on the fused deposition modeling of thermoplastic polymer composites, Compos. B Eng. 201 (2020), 108336, https://doi.org/10.1016/j.compositesb.2020.108336.

[25] A. Nasirov, A. Gupta, S. Hasanov, I. Fidan, Three-scale asymptotic homogenization of short fiber reinforced additively manufactured polymer composites, Compos. B Eng. 202 (2020), 108269, https://doi.org/10.1016/j.compositesb.2020.108269.

[26] M.R. Khosravani, P. Frohn-Sörensen, J. Reuter, B. Engel, T. Reinicke, Fracture studies of 3D-printed continuous glass fiber reinforced composites, Theor. Appl. Fract. Mech. 119 (2022), 103317, https://doi.org/10.1016/j.tafmec.2022.103317.

[27] S. Farah, D.G. Anderson, R. Langer, Physical and mechanical properties of PLA, and their functions in widespread applications — a comprehensive review, Adv. Drug Deliv. Rev. 107 (2016) 367–392, https://doi.org/10.1016/j.addr.2016.06.012.

[28] A.D. Banjo, V. Agrawal, M.L. Auad, A.D.N. Celestine, Moisture-induced changes in the mechanical behavior of 3D printed polymers, Compos. Part C Open Access 7 (2022), 100243, https://doi.org/10.1016/j.jcomc.2022.100243.

[29] T. Dobrescu, N.E. Pascu, G. Jiga, I. Simion, V. Adir, G. Enciu, D.I. Tudose, Tensile behavior of PLA and PLA composite materials under different printing parameters, Mater. Plast. 56 (2019) 783–800, https://doi.org/10.37358/mp.19.4.5268.

[30] H. Dou, Y. Cheng, W. Ye, D. Zhang, J. Li, Z. Miao, S. Rudykh, Effect of process parameters on tensile mechanical properties of 3D printing continuous carbon fiber-reinforced PLA composites, Materials 13 (2020), https://doi.org/10.3390/ma13173850.

[31] A.S. de Moraes, L. de Almeida Furtado, P.H. Maciel Buzzetti, R. de Cássia da Silva, F.S. Semaan, Thermal techniques and their applications: taking advantage of the "heat of the moment, Anal. Chem. Dev. Appl. Challenges Food Anal. (2017) 339–366.

[32] G.H. Heiken, D.T. Vaniman, B.M. French, Lunar Sourcebook: A User's Guide to the Moon, first ed., Press Syndicate of the University of Cambridge, 1991.

[33] IEEE Spectrum, (n.d.). https://spectrum.ieee.org/tech-talk/aerospace/robotic-exploration/china-grew-these-leaves-on-the-moon.

[34] B.M. Tymrak, M. Kreiger, J.M. Pearce, Mechanical properties of components fabricated with open-source 3-D printers under realistic environmental conditions, Mater. Des. 58 (2014) 242–246, https://doi.org/10.1016/j.matdes.2014.02.038.

[35] M. Seggiani, R. Altieri, P. Cinelli, A. Esposito, A. Lazzeri, Thermoplastic blends based on poly(butylene succinate-co-adipate) and different collagen hydrolysates from tanning industry: I—processing and thermo-mechanical properties, J. Polym. Environ. 29 (2021) 392–403, https://doi.org/10.1007/s10924-020-01880-y.

[36] T. Mhlabeni, S. Kesavan Pillai, S.S. Ray, Effect of organically modified layered double hydroxides on the properties of poly(lactic acid)/poly[(butylene succinate)-co-adipate] immiscible blends, J. Appl. Polym. Sci. 137 (2020) 1–10, https://doi.org/10.1002/app.48654.

[37] V. Ojijo, S.S. Ray, R. Sadiku, Effect of nanoclay loading on the thermal and mechanical properties of biodegradable polylactide/poly[(butylene succinate)-co-adipate] blend composites, ACS Appl. Mater. Interfaces 4 (2012) 2395–2405, https://doi.org/10.1021/am201850m.

[38] D. Lascano, L. Quiles-Carrillo, R. Balart, T. Boronat, N. Montanes, Toughened poly (lactic acid)-PLA formulations by binary blends with poly(butylene succinate-co-adipate)-PBSA and their shape memory behaviour, Materials 12 (2019) 1–14, https://doi.org/10.3390/ma12040622.

[39] W. Sachs, V. Meyn, Pressure and temperature dependence of the surface tension in the system natural gas/water, Colloids Surfaces A Physicochem. Eng. Asp. 94 (1995) 291–301.

[40] J.M. Molina, R. Voytovych, E. Louis, N. Eustathopoulos, The surface tension of liquid aluminium in high vacuum: the role of surface condition, Int. J. Adhesion Adhes. 27 (2007) 394–401, https://doi.org/10.1016/j.ijadhadh.2006.09.006.

[41] E. Yousefi, Y. Sun, A. Kunwar, M. Guo, N. Moelans, D. Seveno, Surface tension of aluminum-oxygen system: a molecular dynamics study, Acta Mater. 221 (2021) 9–11, https://doi.org/10.1016/j.actamat.2021.117430.